

Discrete aqueous solvent effects and possible attractive forces*

Y. Burak[†] and D. Andelman[‡]

*School of Physics and Astronomy, Raymond and Beverly Sackler Faculty of Exact Sciences,
Tel Aviv University, Tel Aviv 69 978, Israel*

(July 3, 2000)

We study discrete solvent effects on the interaction of two parallel charged surfaces in ionic aqueous solution. These effects are taken into account by adding a bilinear non-local term to the free energy of Poisson-Boltzmann theory. We study numerically the density profile of ions between the two plates, and the resulting inter-plate pressure. At large plate separations the two plates are decoupled and the ion distribution can be characterized by an effective Poisson-Boltzmann charge that is smaller than the nominal charge. The pressure is thus reduced relative to Poisson-Boltzmann predictions. At plate separations below ~ 2 nm the pressure is modified considerably, due to the solvent mediated short-range attraction between ions in the the system. For high surface charges this contribution can overcome the mean-field repulsion giving rise to a net attraction between the plates.

I. INTRODUCTION

Aqueous ionic solutions are abundant in biological and chemical systems. Often they play a prominent role in determining the properties of charged macromolecules that are immersed in them¹. The mean field theory of electrolytes, known as Poisson-Boltzmann (PB) theory and its linearized version, Debye-Hückel theory¹⁻⁶, are known for many decades and have proved to be useful and important tools. PB theory was applied in the study of colloidal dispersions^{7,8}, biological membranes⁶, synthetic and biological polyelectrolytes^{9,10}, and complex systems such as DNA-lipid complexes¹¹. Nevertheless, PB theory is known to have important limitations. Being a mean field theory, ion-ion correlations are ignored. In addition, the finite size of ions is neglected. These effects have been studied extensively using various approaches¹² such as liquid state¹³⁻¹⁶ and density functional¹⁷ theories, simulations¹⁸⁻²⁰, field theory^{21,22} and other modifications to the PB theory²³⁻²⁶.

Most of the studies of corrections to PB have concentrated on the so-called primitive model, where ions are assumed to interact with each other through the electrostatic interaction and a hard core steric repulsion. Although this model can describe many effects that are neglected in PB theory, it still neglects some physical features that are present in real systems. Most notably, the aqueous solvent is treated as a continuous medium, whereas in reality ions interact with discrete solvent molecules.

Solvent effects are strong especially in water, because the polar water molecules interact very strongly with

ions. The most significant result is that the electrostatic ion-ion interaction is reduced by a factor $\epsilon \simeq 78$ at room temperature, due to screening by the dielectric environment. However the discreteness of the solvent results in a more complicated picture. When ions approach each other at separations of a few water molecular diameters, the effective interaction between them is modified considerably. Fig. 1 shows the correction to the $1/\epsilon r$ potential between two Na^+ ions in water. This effective potential was calculated, using a simulation scheme²⁷, for a bulk NaCl solution of concentration 0.55 M, at room temperature. Note that the short-range potential, remaining after the subtraction of the Coulomb interaction, is oscillatory and predominantly attractive.

The possibility to calculate the effective potential between ions in water leads naturally to the model depicted schematically in Fig. 2. The water is treated as a continuous medium, with a dielectric constant ϵ . In addition to the electrostatic interaction a short-range interaction is included between ion pairs. The short-range potential, denoted as $u_{ij}(r)$, is taken as an input to the model (from simulation), and can in general depend on the ion species i and j . For example, the potential shown in Fig. 1 is used between Na^+ - Na^+ pairs. The effective potential is calculated in a bulk solution and thus depends only on the ion-ion separation. However, systems containing charged surfaces can lead to inhomogeneity or anisotropy in the ion distribution.

The model described above was suggested in Ref. 28, and was studied in planar geometry using the Anisotropic Hyper-Netted Chain (AHNC) approximation¹⁴ in Refs. 29-32. In Ref. 33 we presented

*Submitted to J. Chem. Phys.

[†]email: yorambu@post.tau.ac.il

[‡]email: andelman@post.tau.ac.il

a simplified approach to the same model. In this latter approach, a term accounting for the short-range solvent-mediated ion-ion interaction is added to the PB free energy. The formalism obtained in this way is simple although less accurate than the AHNC approximation, and in particular neglects ion-ion correlations. On the other hand numerical calculations can be done fairly easily, and are feasible in non-planar geometries. In addition, various analytical results can be obtained, and the discrete solvent effects can be readily understood in terms of basic physical principles. In the present paper, which can be regarded as a follow-up of Ref. 33, we use the same formalism to study discrete solvent effects on interacting charged and planar plates.

The outline of the paper is as follows. Section II reviews the model and discusses its application to two charged and planar plates. In Sec. III we discuss the corrections to the PB density profile. In section IV we obtain expressions for the inter-plate pressure and derive a generalized contact theorem. The resulting pressure curves are studied numerically and analytically in section V. Finally, section VI offers some concluding remarks. The technical details in the derivation of the pressure are presented in the Appendix.

II. THE MODEL

A. Free energy

The free energy of the system can be written as a functional of the local ion densities, consisting of the usual PB term and a hydration correction term. Assuming that the boundary conditions are of fixed charges, the following approximated form for the free energy can be obtained³³:

$$\begin{aligned} \Omega = & \frac{\varepsilon}{8\pi} \int (\nabla\Psi)^2 d^3\mathbf{r} + k_B T \int \sum_i c_i \left(\ln \frac{c_i}{\zeta_i} - 1 \right) d^3\mathbf{r} \\ & + \int \Lambda(\mathbf{r}) \left(\nabla^2\Psi + \frac{4\pi}{\varepsilon} \sum_i c_i e_i \right) d^3\mathbf{r} \\ & + \frac{k_B T}{2} \sum_{i,j} \int c_i(\mathbf{r}) c_j(\mathbf{r}') U_{ij}(\mathbf{r} - \mathbf{r}') d^3\mathbf{r} d^3\mathbf{r}' \end{aligned} \quad (1)$$

where Ψ is the electrostatic potential, c_i are the ion densities, e_i are their respective charges, ε is the dielectric constant, $k_B T$ is the thermal energy and U_{ij} is defined below. The bulk ion densities $c_{b,i}$ are determined by the fugacities $\zeta_i = \exp(\beta\mu_i)/\lambda_T^3$, where μ_i are the chemical potentials, λ_T is the de Broglie thermal wave length and $\beta = 1/k_B T$. The simple PB relation $c_{b,i} = \zeta_i$ is altered with the inclusion of hydration interactions, as will be explained below. A detailed discussion of the various approximations involved in Eq. (1) is given in Ref. 33. Here we shall briefly discuss each of the terms, and outline the way in which Eq. (1) is obtained.

The first three terms in Eq. (1) form the usual PB expression for the free energy. The first term is the electrostatic free energy and the second term is the entropy of the ions. The electrostatic potential Ψ is a functional of the ion densities c_i , and is determined by the Poisson equation and the boundary conditions imposed by the surface charges. Instead of writing this dependence explicitly in the free energy, it is convenient to add a third term to Ω , containing a Lagrange multiplier $\Lambda(\mathbf{r})$.

The fourth term in Eq. (1) accounts for the hydration interaction, and is quadratic in the ion densities. The weighted potential U_{ij} is defined as:

$$U_{ij} = 1 - e^{-\beta u_{ij}(|\mathbf{r}-\mathbf{r}'|)} \quad (2)$$

where u_{ij} is the nominal short-range hydration interaction between ions of species i and j . To obtain Eq. (1) we first treat the short-range interaction u_{ij} using a virial expansion of the grand canonical potential, keeping terms up to the quadratic order. The electrostatic interaction is then treated exactly as in PB theory, using a mean field approximation for the electrostatic potential Ψ . As an alternative approach Eq. (1) can be obtained from a field theory expansion of the grand partition function³⁴.

B. Density equations

The density profiles are obtained by minimizing the free energy Ω with respect to the ion densities c_i . The third term in Eq. (1), containing the Lagrange multiplier $\Lambda(\mathbf{r})$ allows us to regard the densities $c_i(\mathbf{r})$ and the electrostatic potential $\Psi(\mathbf{r})$ as independent fields, and require that Ω has an extremum with respect to the three fields c_i , Ψ and Λ . Requiring that Ω has an extremum with respect to Ψ gives:

$$\Lambda = \frac{\varepsilon}{4\pi} \Psi \quad (3)$$

and the extremum condition with respect to c_i then gives:

$$\ln \frac{c_i(\mathbf{r})}{\zeta_i} + \sum_j \int c_j(\mathbf{r}') U_{ij}(\mathbf{r} - \mathbf{r}') d^3\mathbf{r}' + \beta e_i \Psi(\mathbf{r}) = 0 \quad (4)$$

where relation (3) has been substituted to express Λ in terms of Ψ . This equation is supplemented by the Poisson equation:

$$\nabla^2\Psi = -\frac{4\pi}{\varepsilon} \sum_i e_i c_i \quad (5)$$

Since Eq. (4) is an integral equation, the c_i cannot be written as a simple function of Ψ . Therefore a single equation for Ψ , analogous to the PB equation, cannot be obtained, and we are left with the two coupled equations (4) and (5). These equations should be solved together

to obtain the electrostatic potential and density profiles. For $U \rightarrow 0$, Eq. (4) reduces to the Boltzmann equation $c_i = \zeta_i \exp(-\beta e_i \Psi)$. In the bulk $\Psi = 0$, leading to the relation $c_{b,i} = \zeta_i$. Combining these relations with Eq. (5) reproduces the PB equation:

$$\nabla^2 \Psi = -\frac{4\pi}{\varepsilon} \sum_i c_{b,i} e_i e^{-\beta e_i \Psi} \quad (\text{PB}) \quad (6)$$

Equations (4) and (5) were solved for a single charged and planar plate in Ref. 33. The treatment of two parallel plates is very similar, and is outlined below for completeness. The system is shown schematically in Fig. 2b. The plate positions are designated by $z = 0$ and $z = d$, using the convention that these are the coordinates of closest approach of the ions to the plates (while the potentials $u_{ij}(r)$ are measured from the *centers* of the ions). The two plates are negatively charged, each one with a uniform surface charge σ . No discreteness of surface charge is taken into account in the present work. We assume an electrolyte of valency $z_+ : z_-$, *i.e.*, a solution of positive and negative ions of charges $e_{\pm} = \pm z_{\pm} e$, where e is the electron charge.

In order to simplify the equations further, the interactions between the different pairs of ion species can be taken to be equal, *i.e.*, $U_{ij}(\mathbf{r}) = U_{++}(\mathbf{r}) \equiv U(\mathbf{r})$ where U_{++} is the weighted potential between the (positive) counterions. The exact choice of U_{+-} and U_{--} is expected to be of only minor significance, as the co-ions are repelled from the surface neighborhood and only the positive counterions reach high densities there. From charge neutrality we have $c_b \equiv c_{b,+} = (z_-/z_+)c_{b,-}$ and similarly $\zeta \equiv \zeta_+ = (z_-/z_+)\zeta_-$, where the relation between c_b and ζ will be determined later.

Due to the one-dimensional symmetry imposed by the charged and planar planes, the integration in Eq. (4) can be performed over the $x - y$ plane to obtain:

$$c_{\pm}(z) = \zeta_{\pm} e^{\mp \beta e z_{\pm} \Psi} \exp \left[-\int_0^d c(z') B(z - z') dz' \right] \quad (7)$$

where $c = c_+ + c_-$ is the total ion density and $B(z)$ is the effective interaction between two layers of ions, expressed as an integral of $U(\mathbf{r})$ in the plane of constant z . Using cylindrical coordinates:

$$B(z) = 2\pi \int_0^{\infty} \rho d\rho U(\sqrt{z^2 + \rho^2}) \quad (8)$$

The Poisson equation (5) reads:

$$\frac{d^2 \Psi}{dz^2} = \frac{4\pi e}{\varepsilon} \zeta_{z_+} (e^{\beta e z_- \Psi} - e^{-\beta e z_+ \Psi}) \times \exp \left[-\int_0^d c(z') B(z - z') dz' \right] \quad (9)$$

Equations (7) and (9) are supplemented by the following boundary conditions:

$$\left. \frac{d\Psi}{dz} \right|_{z=0} = -\frac{4\pi}{\varepsilon} \sigma \quad ; \quad \left. \frac{d\Psi}{dz} \right|_{z=d/2} = 0 \quad (10)$$

since the problem with two plates of equal charge at $z = 0$ and $z = d$ of equal charge is symmetric about the mid-plane $z = d/2$.

Finally, the relation between ζ and the bulk density c_b can be obtained from Eq. (7). We imagine that the two plates are immersed in a bath of electrolyte. In the region outside the plates an equation similar to Eq. (7) holds, where the integration inside the exponent is performed in the external region. Far away from the plates, as Ψ becomes zero, c_+ and c_- assume their asymptotic constant, bulk values. The integrand inside the exponential can be replaced by $-(1 + z_+/z_-)c_b B(z - z')$ leading to the result:

$$c_b = \zeta \exp \left[-\left(1 + \frac{z_+}{z_-}\right) B_t c_b \right] \quad (11)$$

where:

$$B_t \equiv \int_{-\infty}^{\infty} dz B(z) = \int d^3 \mathbf{r} U(\mathbf{r}) \quad (12)$$

is also equal to $2B_2$, the second virial coefficient. The limit $B_t c_b \rightarrow 0$ is the limit in which the short-range interaction becomes negligible in the bulk. In this limit the relation between the bulk density and fugacity of Eq. (11) tends to the ideal gas relation $c_b = \zeta = \exp(\beta\mu)/\lambda_T^3$.

In the next section we will concentrate on a symmetric 1 : 1 electrolyte, where the equations (7) and (9) take the form:

$$c_{\pm}(z) = \zeta e^{\mp \beta e \Psi} \exp \left[-\int_0^d c(z') B(z - z') dz' \right] \\ \frac{d^2 \Psi}{dz^2} = \frac{8\pi e}{\varepsilon} \zeta \sinh(\beta e \Psi) \times \exp \left[-\int_0^d c(z') B(z - z') dz' \right] \quad (13)$$

and:

$$c_b = \zeta \exp(-2B_t c_b) \quad (14)$$

C. Definitions and parameters

For the short-range ion-ion potential $u(\mathbf{r} - \mathbf{r}')$ we use the effective potential between $\text{Na}^+ - \text{Na}^+$ ion pairs, shown in Fig. 1. For ion-ion separations below 2.9\AA a hard core interaction is assumed. Fig. 3 shows the effective layer-layer interaction $B(z)$, as was derived from this potential using Eq. (8). This effective interaction is mostly attractive, as $B(z)$ is negative on most of its range, and has a characteristic range of approximately

7 Å. The structure of $B(z)$ reflects the oscillatory behavior of $u(\mathbf{r})$.

It is useful to introduce the length scales characterizing the PB density profiles⁶. The *Gouy-Chapman length*, defined as $b = \epsilon k_B T / (2\pi e |\sigma|)$, characterizes the width of the diffusive counterion layer close to a single charged plate with a surface charge density σ , in the absence of added salt. The *Debye-Hückel screening length*, $\lambda_D = (8\pi c_b e^2 / \epsilon k_B T)^{-1/2}$, equal to 19.6 Å for $c_b = 0.025$ M at room temperature characterizes the decay of the screened electrostatic interaction in a solution with added salt. The strength of the electrostatic interaction can also be expressed using the *Bjerrum length*, $l_B = e^2 / (\epsilon k_B T)$. This is the distance at which the electrostatic interaction between two unit charges in a dielectric medium becomes equal to the thermal energy. It is equal to about 7 Å in water at room temperature. In terms of the Bjerrum length $b = e / 2\pi l_B |\sigma|$ and $\lambda_D = (8\pi c_b l_B)^{-1/2}$.

The inclusion of the hydration interaction introduces additional length scales in the system. For the interaction of Figs. 2 and 3, the range of the interaction d_{hyd} is approximately 7 Å, over twice the hard core diameter $d_{\text{hc}} = 2.9$ Å. The strength of the hydration interaction is characterized by the second virial coefficient $B_t/2$, with $B_t \simeq -(7.9 \text{ Å})^3$ as is calculated from Eq. (12).

III. DENSITY PROFILES

Equations (7) and (9) are a set of three nonlinear integrodifferential equations. We treat them numerically using an iterative scheme, based on the assumption that the positive ion density profile is dominated by the electrostatic interaction. We start with the PB profile and calculate iteratively corrections to this profile, as result from Eqs. (7) and (9). For a 1:1 electrolyte we iteratively solve the equation:

$$\frac{d^2 \Psi^{(n)}}{dz^2} = \frac{8\pi e}{\epsilon} \zeta \sinh(\beta e \Psi^{(n)}) \times \exp \left[- \int_0^d c^{(n-1)}(z') B(z-z') dz' \right] \quad (15)$$

where the superscript n stands for the n th iteration,

$$c_{\pm}^{(n)}(z) \equiv \zeta e^{\mp \beta e \Psi^{(n)}} \times \exp \left[- \int_0^d c^{(n-1)}(z') B(z-z') dz' \right] \quad (16)$$

and the zeroth order densities $c_{\pm}^{(0)}$ are taken as the density profiles generated by the PB equation (6). The boundary conditions (10) are satisfied by the electrostatic potential in all iterations. The solution converges after several iterations. It is interesting to note that the first iteration captures most of the effect. This observation can lead to

various analytical results, as shown in Ref. 33 for a single plate.

In the following sections we will concentrate on the pressure between the plates. First we discuss briefly the modification to the PB density profiles. Let us begin by considering a large plate separation d . In this case the results are similar to the single-plate case, since d is larger than all other length scales in the system, and we present them for completeness.

Fig. 4 shows the density profile of the positively charged counterions (solid line) between two charged plates, with $d = 50$ Å. Only one half of the system is shown, since the profile is symmetric around the mid-plane. The surface charge, $|\sigma| = 0.333$ C/m² corresponds to approximately 48 Å² per unit charge. This is a typical high surface charge obtained for mica plates. It corresponds to a Gouy-Chapman length $b = 1.06$ Å, at a temperature of 298 K, with $\epsilon = 78$. The electrolyte bulk concentration is 0.025 M, corresponding to a Debye-Hückel screening length $\lambda_D = 19.58$ Å. The density profile is compared to the result of PB theory (dotted line).

The main effect is that the short-range attraction draws additional counterions to the vicinity of the charged plate. Note, however, that the contact density remains very close to the PB density, as will be explained later. The increase of the counterion density near the plate is followed by a depletion further away. This can be understood in the no-salt case since the total number of counterions is fixed. In our case the salt concentration is low. The Debye-Hückel screening length is large compared to the Gouy-Chapman length and compared to the range of the short-range interaction, so the salt has a minor effect.

The counterion density profile is also compared with results of the AHNC approximation³⁵ that were obtained using the same short-range hydration potential ('x' symbols). The qualitative effect is similar in our model and in the AHNC. Specifically, both density profiles follow the PB density curve for the first few Angströms from the plate and show a considerable decrease in the positive ion density, relative to PB, starting at a distance of about 5 Å from the plate. The maximal decrease in the density is approximately 30% in our model and almost 50% in the AHNC profile, both relative to the PB profile.

The effect of the short-range ion-ion interaction strongly depends on the surface charge. This is demonstrated in Fig. 5. The ratio of the counterion density and its PB value, c/c^{PB} , is shown for three values of σ . The effect of the hydration potential is very minor for small surface charge ($|\sigma| = 0.0333$ C/m² $\simeq 1 e / 480$ Å²), where the ratio c/c^{PB} is approximately 2% at its maximum, and considerable for a surface charge of 0.333 C/m² = 1 e / 48 Å², where it reaches approximately 40%.

As the plate separation decreases, the modification to c^{PB} is expected to remain similar to the single plate case as long as $d/2$ is large compared to b and to d_{hyd} . This can indeed be seen in Fig. 6, where a high surface charge,

as in Fig. 4, is considered. In this case $b \ll d_{\text{hyd}}$, so a deviation from the single plate curve is expected when $d/2 \lesssim d_{\text{hyd}} \simeq 7 \text{ \AA}$. The ratio c/c_{PB} is shown for several plate separations between 5 and 50 \AA . The results are very similar for $d = 50, 35$ and 20 \AA (Fig. 6a). In particular, note that the contact density remains very close to the PB value in all three separations. This is a result of the generalized contact theorem, derived in section IV. For smaller d , 5 and 10 \AA (Figures 6b and 6c, respectively) the behavior is different, and in particular the contact density deviates from the PB value. The effect of decreasing d was found to be similar for smaller surface charge (*e.g.*, 0.1 C/m².) and for salt concentration up to 0.1 M.

The most important effect on the density profile is that the ion density is depleted far away from the charged plates. When the two plates are highly separated from each other the ion density can be described, far away from the plates, using an effective PB surface charge. This effective charge was calculated in Ref. 33, and is smaller than the nominal charge (for example, for the surface charge used in Fig. 4 it is smaller by a factor of ~ 3.8). The reduced density leads to a reduced pressure, relative to PB, as will be explained in the following sections.

IV. PRESSURE EQUATION AND CONTACT THEOREM

The pressure P_{in} in the region between the two plates can be obtained by differentiating the free energy Ω with respect to the plate separation d :

$$P_{\text{in}} = -\frac{\delta\Omega}{\delta d} \quad (17)$$

To compute $\delta\Omega$ we can imagine that a ‘slice’ of width δd is inserted at some position z_0 between the two plates. Adding up all the contributions to $\delta\Omega$, and using Eq. (7) and the boundary conditions (10) we obtain:

$$P_{\text{in}} = k_B T \sum_i c_i(z_0) - \frac{\varepsilon}{8\pi} \left(\frac{d\Psi}{dz} \right)^2 \Big|_{z_0} - k_B T \sum_{ij} \int_0^{z_0} dz \int_{z_0}^d dz' c_i(z) c_j(z') \frac{dB}{dz}(z' - z) \quad (18)$$

This result is correct for any combination of ion species i , assuming the same short-range interaction u_{ij} between different ion pairs. The full derivation is given in the Appendix. The pressure is equal throughout the plate spacing and, therefore, independent on the choice of z_0 .

The net pressure P between the plates is the difference between the pressure inside and outside the plates. The latter is equal throughout the region outside the plates. In particular, it is equal to the bulk pressure P_{bulk} , so we have:

$$P = P_{\text{in}} - P_{\text{bulk}} \quad (19)$$

To obtain P_{bulk} , we note that an equation similar to Eq. (18) holds in the bulk, with constant electrostatic potential and with c_i constant and being equal to the bulk densities. For the case of a 1:1 electrolyte, we find:

$$P_{\text{bulk}} = 2k_B T c_b (1 + B_t c_b) \quad (20)$$

Since B_t is negative the bulk pressure is lower than its PB value. Note that in the case of no added salt $P_{\text{bulk}} = 0$.

The expression (18) assumes a particularly simple form if we set z_0 to zero, namely on one of the plates. Then the third term in (18) vanishes and the second term is fixed by the boundary conditions, giving:

$$P = k_B T \sum_i c_i(0) - \frac{2\pi}{\varepsilon} \sigma^2 - P_{\text{bulk}} \quad (21)$$

Alternatively, if we choose z_0 at the mid-plane, $z = d/2$, by symmetry the second term in (18) vanishes and the pressure is expressed as:

$$P = k_B T \sum_i c_i(d/2) - k_B T \sum_{ij} \int_0^{d/2} dz \int_{d/2}^d dz' c_i(z) c_j(z') \frac{dB}{dz}(z' - z) - P_{\text{bulk}} \quad (22)$$

The equality of these two expressions for the pressure results in the generalized contact theorem^{1,36}:

$$\sum_i c_i(0) = \frac{2\pi\beta}{\varepsilon} \sigma^2 + \sum_i c_i(d/2) - \sum_{ij} \int_0^{d/2} dz \int_{d/2}^d dz' c_i(z) c_j(z') \frac{dB}{dz}(z' - z) \quad (23)$$

The very small relative change of the contact density, compared to PB theory, at large plate separations can be understood from this result. We consider first the case of high surface charge, where the Gouy-Chapman length is small compared to the Debye-Hückel screening length, $b \ll \lambda_D$. In this case the second and third terms on the right hand side of Eq. (23) become negligible compared to the first term when $d \gg b, d_{\text{hyd}}$, where d_{hyd} is the range of the hydration interaction. The contact ion density is then dominated by the positive ion density, and is very close to the PB value. When there are only counterions in the solution and $d \rightarrow \infty$ (or equivalently, in the case of one isolated plate), we have exactly, as in PB theory :

$$c_+(0) = \frac{2\pi\beta}{\varepsilon} \sigma^2 \quad (\text{one plate, no salt}) \quad (24)$$

If b is not small compared to λ_D , the correction to the contact density is still small for large enough plate separations, assuming that the hydration interaction is negligible in the bulk, *i.e.* $-B_t c_b = -B_t / (8\pi l_B \lambda_D^2) \ll 1$.

When $d \gg \lambda_D$ and $d > d_{\text{hyd}}$, the coupling between the two plates is negligible and Eq. (23) becomes:

$$\sum_i c_i(0) \simeq \frac{2\pi\beta}{\varepsilon} \sigma^2 + P_{\text{bulk}} \quad (25)$$

The only difference in this expression relative to the PB contact density is the change in the bulk pressure. This change is negligible if the hydration interaction is negligible in the bulk.

For smaller d , the integral in (23) can contribute to a significant change in the contact density relative to PB theory. This can be seen in Fig. 6, where $b \ll \lambda_D$, at plate separations below $\sim 10 \text{ \AA}$.

V. PRESSURE CURVES

A. Pressure beyond Poisson-Boltzmann

Using equations (22) and (20) the pressure can be written in our model as the sum of the following three terms:

$$\begin{aligned} P &= k_B T \sum_i [c_i(d/2) - c_{b,i}] \\ &- k_B T \sum_{ij} \int_0^{d/2} dz \int_{d/2}^d dz' c_i(z) c_j(z') \frac{dB}{dz}(z' - z) \\ &- 2k_B T B_t c_b^2 \end{aligned} \quad (26)$$

A symmetric 1:1 electrolyte is assumed for simplicity throughout this section. We would like to compare this pressure with the PB pressure, which can be written as follows:

$$P_{\text{PB}} = k_B T \sum_i [c_{\text{PB},i}(d/2) - c_{b,i}] \quad (27)$$

where $c_{\text{PB},i}(d/2)$ is the PB density of the i th ion species at the mid-plane. The first term in Eq. (26),

$$P_m = k_B T \sum_i [c_i(d/2) - c_{b,i}] \quad (28)$$

is similar in form to the PB pressure (27), but the mid-plane density in equations (28) and (27) can be different. The second term in Eq. (26), which we denote as the hydration pressure:

$$P_{\text{hyd}} = -k_B T \sum_{ij} \int_0^{d/2} dz \int_{d/2}^d dz' c_i(z) c_j(z') \frac{dB}{dz}(z' - z) \quad (29)$$

is the integrated short-range force acting between ion pairs in the two halves of the system. The third term is the change in the bulk pressure relative to PB theory, due to the inclusion of a 2nd virial coefficient in the bulk equation of state.

Some simple observations can be made immediately from Eq. (26). These observations will be useful in the next subsection, where the numerically calculated pressure curves are presented (Figs. 7 and 8). For now let us assume that the third term in Eq. (26) is negligible as compared to the first two. Of these two terms, the first, P_m , is linear in the density whereas the second term, P_{hyd} , is quadratic. As a result, the relative importance of P_m and P_{hyd} depends on the plate separation d . At large d the density in the mid-plane region is small, so that $P_{\text{hyd}} \ll P_m$. The main correction to the PB pressure (27) then comes from the change of the mid-plane density, $c(d/2) - c_{\text{PB}}(d/2)$. Far away from the two plates the system behaves as predicted by PB theory with a modified, effective surface charge. The mid-plane density is depleted relative to PB, since counterions are attracted to the vicinity of the charged plates. Hence the pressure is smaller than in PB theory. As the plate separation decreases and the mid-plane density increases, P_{hyd} can become important.

B. Numerical results

The general arguments of the previous section can be verified by calculating numerically the pressure using Eq. (26). Fig. 7 shows the pressure as a function of the plate separation d for a surface charge $|\sigma| = 0.333 \text{ C/m}^2 \simeq 1 e/48 \text{ \AA}^2$ and bulk ion density $c_b = 0.025\text{M}$ (solid line). The pressure is compared with P_{PB} (dotted line). The contribution of P_m , the first term in Eq. (26), is also shown (dashed line).

The behavior of the pressure at a large range of plate separations is shown in Fig. 7a on a semi-logarithmic plot. At large d , the pressure is dominated by P_m , as expected. It is considerably smaller than the PB pressure, due to the reduced effective charge on the plates. At lower d the second term in Eq. (26), P_{hyd} , becomes dominant, and the overall interaction is attractive at plate separations between 6 and 12 \AA . Note that the apparent sharp decrease in the pressure at a separation of approximately 13 \AA is artificial, and results from the divergence of the logarithmic scale as the pressure approaches zero. Fig. 7b shows the same pressure using a linear scale, in the region in which it becomes negative (attractive). The net pressure crosses smoothly from positive to negative values due to a steady increase in the magnitude of the (negative) P_{hyd} . At very short separations P_m dominates again, and the pressure coincides with the predictions of PB theory.

Fig. 8 shows the effect of the hydration potential for a smaller surface charge, $|\sigma| = 0.119 \text{ C/m}^2 \simeq 1 e/135 \text{ \AA}^2$. In this case and for all surface charge, $|\sigma| \lesssim 0.25 \text{ C/m}^2$, the pressure is repulsive at all plate separations. The correction over the PB result is much smaller than in Fig. 7, but still significant. At plate separations of approximately 5 to 20 \AA P_{hyd} is the dominant contribution

to the deviation from PB, and results in a considerably reduced pressure. At larger d the pressure is reduced mainly because of the change in the mid-plane density.

C. Comparison with AHNC

Fig. 9 shows a comparison of the pressure obtained in our model (a) and in the AHNC approximation³⁷ (b), at surface charge $|\sigma| = 0.333 \text{ C/m}^2 \simeq 1 e/48 \text{ \AA}^2$. The same short-range hydration potential is used in the two calculations. The main plots show the pressure using a logarithmic scale. The insets show the pressure on a linear scale in the region where it becomes attractive. The full pressure (solid line) is compared in Fig. 9a with the PB pressure (dotted line). In Fig 9b the AHNC pressure (solid line) is compared with the pressure obtained using an electrostatic and hard core interaction only (dotted line). Since the AHNC approximation accounts for ion-ion correlations, there are differences between the pressure curves in our model as compared to the AHNC approximation. However a comparison of Figs. 9a and 9b shows that very similar qualitative and even semi-quantitative effects of the hydration interaction are found in the two calculations.

A comparison for smaller $|\sigma| = 0.119 \text{ C/m}^2 \simeq 1 e/135 \text{ \AA}^2$ is shown in Fig. 10. The solid line is the pressure in our model and the dashed line is the AHNC pressure. The dotted line shows the PB pressure. As in Fig. 9, the qualitative effect is similar in the two calculations.

Since the AHNC approximation takes into account ion-ion correlations, the comparison allows us to assess the relative importance of correlations and discrete solvent effects. The results shown in Figs. 7 and 9 indicate that discrete solvent effects can be much larger than correlation effects induced by the electrostatic interaction. For smaller surface charge, as in Figs. 8 and 10, these effects are of similar order of magnitude. In the AHNC approximation the pressure includes an electrostatic term due to correlations between ions in the two halves of the system, in addition to the hydration and mid-plane density contributions. In Fig. 10 this term is of similar order of magnitude as P_{hyd} , and is the main source for the difference between the solid line (our model) and dashed line (AHNC). For larger surface charge, as in Fig. 9, P_{hyd} becomes much larger than the electrostatic contribution.

When divalent ions are present in the solution, correlation effects become much larger than in the monovalent case^{18,19}. Discrete solvent effects are also modified, since the effective short-range interaction between two divalent ions is different in the two cases. When the charge on the ions is doubled, the electrostatic interaction between two ions increases by a factor of 4. The ion-ion separation where the electrostatic interaction is equal to $k_B T$ increases from $l_B \simeq 7 \text{ \AA}$ to almost 30 \AA . On this electrostatic scale, the water molecular size ($\sim 3 \text{ \AA}$) is

much smaller than in the monovalent case. Hence we can expect the solvent to be more similar to a continuous dielectric medium. Indeed, the correction to the $1/\epsilon r$ potential between two (artificial) Na^{2+} ions in water³⁸ is found to be purely repulsive, and is significant only at separations below $\sim 10 \text{ \AA}$, where the electrostatic interaction is considerably larger than $k_B T$. Thus we expect discrete solvent effects to be less important than correlations in the divalent case.

D. Further analysis

1. Large plate separations

As discussed above, the hydration term becomes small at large d , compared to the change in the mid-plane density. In order to study the contribution of the mid-plane density to the pressure, let us assume that the plate separation d is much larger than all other length scales in the system: $b, d_{\text{hyd}}, \lambda_D$. The two plates are then decoupled and the mid-plane potential can be written as $\Psi(d/2) \simeq 2\Psi_1(d/2)$ where $\Psi_1(d/2)$ is the electrostatic potential at a distance $d/2$ from a *single* plate. We assume also that $\lambda_D \gg b$, which is usually the case when the surface charge density is large. At a large distance from the plate the single plate profile is a PB profile, corresponding to a renormalized surface charge σ_{eff} ³³. The contribution P_m to the pressure can then be written as follows⁶:

$$P_m \simeq \frac{8k_B T}{\pi l_B \lambda_D^2} \left(1 - \frac{2b_{\text{eff}}}{\lambda_D}\right) e^{-d/\lambda_D} \quad (30)$$

where $b_{\text{eff}} = 1/2\pi l_B |\sigma_{\text{eff}}|$ is the effective Gouy-Chapman length. A similar expression holds for the PB pressure, with the nominal Gouy-Chapman length b used instead of b_{eff} . We thus find that:

$$\frac{P_m}{P_{\text{PB}}} \simeq \frac{1 - 2b_{\text{eff}}/\lambda_D}{1 - 2b/\lambda_D} \simeq 1 - 2\frac{b_{\text{eff}} - b}{\lambda_D} \quad (31)$$

In Ref. 33 an analytical expression for $b_{\text{eff}} - b$ is found. Its general behavior is:

$$b_{\text{eff}} - b \sim -\frac{B_t}{l_B b} \quad (32)$$

with a numerical prefactor of $1/12\pi$ in the limit $b \ll d_{\text{hyd}}$ and a numerical prefactor $1/4\pi$ in the limit $b \gg d_{\text{hyd}}$. The parameters of the hydration interaction $d_{\text{hyd}} \simeq 7 \text{ \AA}$ and $B_t \simeq -500 \text{ \AA}^3$ are as defined in Sec. II C.

A careful treatment of Eq. (26) shows that the second and third terms also add a contribution to the pressure that should be regarded as linear in the density, although this contribution is small. For large enough d the integration range in the second term of Eq. (26) can be extended to be between $-\infty$ and $+\infty$ because dB/dz has a finite range. In addition all quantities can be replaced by their

mid-plane values. We then find that the second and third terms of Eq. (26) give:

$$\begin{aligned}
& -k_B T \sum_{ij} \int_0^{d/2} dz \int_{d/2}^d dz' c_i(z) c_j(z') \frac{dB}{dz}(z' - z) \\
& - 2k_B T B_t c_b^2 \\
& \simeq \frac{1}{2} k_B T B_t \sum_{ij} [c_i(d/2) - c_b][c_j(d/2) - c_b] \\
& + 2k_B T B_t c_b \sum_i [c_i(d/2) - c_b] \quad (33)
\end{aligned}$$

The first term is quadratic in $[c_i(d/2) - c_b]$ and can be neglected relative to P_m at large d . The second term is linear, although small because $B_t c_b \ll 1$. It accounts for the small difference between the dashed and solid lines at large d in Fig. 7a.

2. Hydration pressure

The behavior of P_{hyd} , the hydration pressure term, can be understood as follows. As a zero-th order approximation, the ion density is dominated by electrostatics and can be replaced in Eq. (29) by its PB value. Fig. 11 shows that this gives a very good approximation. Hence we can write:

$$P_{\text{hyd}} \simeq \sum_{ij} \int_0^{d/2} dz \int_{d/2}^d dz' c_{\text{PB},i}(z) F(z' - z) c_{\text{PB},j}(z') \quad (34)$$

where

$$F(z) \equiv -k_B T \frac{dB(z)}{dz} \quad (35)$$

represents the force between two planar ion layers separated by a distance z . The following behavior of $F(z)$ can be inferred from Fig. 3. At inter-layer separations $z < d_{\text{hc}} = 2.9 \text{ \AA}$ $F(z)$ is positive (repulsive). At larger z the value of $B(z)$ increases from its large negative value at $z = d_{\text{hc}}$ to zero over a few Angströms, leading to a strongly attractive (negative) $F(z)$. A closer inspection of Fig. 3 shows that $F(z)$ is oscillatory, due to the local maxima and minima of $B(z)$. As we shall see below these fine details are smoothed away when two diffusive layers of finite thickness interact.

The behavior of P_{hyd} in Fig. 11 can now be understood as follows. Most of the counterions are concentrated near the two plates, in layers whose thickness is of order $b = 1.06 \text{ \AA}$. Note that b is small compared to $d_{\text{hyd}} \simeq 7 \text{ \AA}$. When $d > d_{\text{hyd}}$ these two layers do not interact directly with each other through the short-range interaction. Ions in the two sides of the mid-plane interact with each other, leading to a negative (attractive) P_{hyd} . As d is decreased towards d_{hyd} , larger and larger ion densities come into

contact through $F(z)$ and the magnitude of the negative P_{hyd} increases accordingly. The gradual increase in the magnitude of P_{hyd} reflects the algebraic decay of the density profile near each layer. When d decreases below $\sim 2d_{\text{hyd}} \simeq 14 \text{ \AA}$, the magnitude of P_{hyd} increases more rapidly, as the ions in the two layers interact with ions in the mid-plane region.

The behavior of P_{hyd} changes when d decreases below d_{hyd} . Most of the contribution to P_{hyd} now comes from the interaction between the dense counterion layers near the two plates. As d decreases these layers are separated by correspondingly decreasing distances. The hydration pressure follows roughly the structure of $F(z)$. It is strongly attractive for $d \gtrsim d_{\text{hc}}$ and repulsive for $d < d_{\text{hc}}$. The fine details of $F(z)$ are smoothed due to the thickness of the diffusive ion layers.

As the plate separation decreases below d_{hc} towards contact P_{hyd} tends to zero, as it should since $F(0) = -k_B T \left. \frac{dB}{dz} \right|_{z=0} = 0$. One implication of this result is that P_m returns to be the dominant contribution to the pressure, even for high surface charges. Another implication is that the short-range interaction becomes unimportant. As in PB theory, the ions in the region between the two plates become essentially a confined ideal gas, and their total number is determined by charge neutrality. Thus P_m coincides with the PB pressure matching the *nominal* surface charge density σ . This is seen clearly in Fig. 7.

3. Small plate separations

In experiments the actual surface charge is usually not exactly known, because the number of ions dissociating from the surface is uncontrolled. The PB charge is then fitted to the large separation behavior. This charge can be significantly smaller than the actual surface charge, as discussed above. The interpretation of our results is then as follows. At plate separations below approximately 2 nm, an attractive force appears, due to P_{hyd} . This force can reduce the net repulsion, or even induce a net attraction, depending on the surface charge on the plates. As the plate separation decreases below the range of the hydration interaction $d_{\text{hyd}} \simeq 7 \text{ \AA}$, P_{hyd} decreases and eventually tends to zero. The pressure then coincides with the PB pressure matching the *nominal* surface charge. As was pointed out in Ref. 28 this leads to an apparent strong repulsive force when compared with the PB curve fitted to the large separation behavior. As an example, the pressure corresponding to $\sigma = 0.25 \text{ C/m}^2 \simeq 1 e/64 \text{ \AA}^2$ is shown in Fig. 12 as a function of d (solid line) using a linear scale. The dashed line shows the PB pressure curve using an effective surface charge chosen to match the large d behavior of the solid line. When the two lines are compared a strong (apparent) repulsive contribution is seen in the solid line below $d \simeq 5 \text{ \AA}$, and an attractive contribution is seen for $5 \text{ \AA} \lesssim d \lesssim 15 \text{ \AA}$.

VI. CONCLUDING REMARKS

Summarizing our results on the pressure, we find that hydration effects can be understood as arising from two contributions. The first contribution is the change in the mid-plane ion density. This contribution dominates at large plate separations and can be understood in terms of an effective PB surface charge in our model. The effective PB charge is smaller than the nominal charge due to the accumulation of counterions in the vicinity of the charged plates. Thus the pressure is reduced relative to PB theory, using the same surface charge.

As an alternative viewpoint, the PB surface charge can be chosen to match the large plate separation of the pressure in our model. When this is done, an apparent repulsive force appears in our model at very small plate separations ($\lesssim 5 \text{ \AA}$), as compared with the fitted PB pressure.

The second contribution to the pressure is the direct solvent mediated attraction between ion pairs in the two halves of the system. This latter term can become dominant at plate separations between $\sim 0.5 \text{ nm}$ and $\sim 2 \text{ nm}$. It can induce a net attractive interaction between the two plates when the surface charge is high.

Attraction between like-charged surfaces is never predicted by PB theory^{39,40}. On the other hand, mechanisms involving correlations can lead to attraction. Several approaches have shown that ion-ion correlations can have this effect, in the framework of the primitive model¹⁷⁻¹⁹. In practice, this attraction can be strong enough to overcome the mean field repulsion when divalent ions are present in the solution. When there are only monovalent ions in the solution, ion-ion correlations have a much smaller effect. Another mechanism that can lead to attraction is the van der Waals force, arising from correlations between the polarizations on the two surfaces. As we find in this work, solvent mediated forces, related to ion-solvent correlations, are another mechanism that can induce inter-surface attraction. In some cases (monovalent ions, small separation, large surface charge) they are the leading mechanism for attraction.

A strong deviation from PB predictions is indeed measured^{41,42} between charged surfaces in aqueous solution at separation below $\sim 2 \text{ nm}$. The force includes an oscillatory contribution, with a period corresponding to the water molecular size. This force is due to the structuring of water in layers between the surfaces. In addition to this oscillatory contribution, an additional strong contribution is seen, which is often referred to as the hydration force^{1,41}. The aqueous pair potential model of Ref. 28 was a first step towards the understanding of this force. A more realistic picture will probably emerge if a proper effective ion-surface interaction will be included, in addition to the effective ion-ion interaction. In addition, the modification to the ion-ion effective potential in a confined geometry may also be important. In order to assess the importance of these effects, further simulation results are needed as an input to the model.

The aqueous pair potential and the free energy (1) involve various approximations, which are discussed extensively in Refs. 33,43. Nevertheless, the large modification to the PB pressure, as obtained also using the AHNC approximation^{31,32,35}, indicates that the solvent effects on the ion distribution are a crucial ingredient in the origin of hydration forces^{28,44}. The semi-quantitative agreement of our results with the AHNC approximation indicates that our formalism captures the important effects and suggests its further application in non-planar geometries, where the AHNC approximation is not applicable.

ACKNOWLEDGMENTS

We wish to thank S. Marčelja for numerous valuable discussions and for sharing with us his results prior to publication. Partial support from the U.S.-Israel Binational Foundation (B.S.F.) under Grant No. 98-00429, and the Israel Science Foundation founded by the Israel Academy of Sciences and Humanities - Centers of Excellence Program is gratefully acknowledged.

APPENDIX A: DERIVATION OF THE PRESSURE

The free energy of the system is given by the sum: $\Omega = \Omega_{\text{PB}} + \Delta\Omega$ with Ω_{PB} and $\Delta\Omega$ defined as follows:

$$\begin{aligned} \Omega_{\text{PB}} &= \frac{\varepsilon}{8\pi} \int_0^d \left(\frac{d\Psi}{dz} \right)^2 dz + k_B T \int_0^d \sum_i c_i \left(\ln \frac{c_i}{\zeta} - 1 \right) dz \\ \Delta\Omega &= \frac{1}{2} k_B T \sum_{i,j} \int_0^d dz \int_0^d dz' c_i(z) c_j(z') B_{ij}(z' - z) \end{aligned} \quad (\text{A1})$$

We now imagine that the separation between the two plates is increased from d to $d + \delta z$ by adding a ‘slice’ of width δz between the planes z_0 and $z_0 + \delta z$. We map the regions $0 \leq z \leq z_0$ and $z_0 \leq z \leq d$ in the original system to the regions $0 \leq z \leq z_0$ and $z_0 + \delta z \leq z \leq d + \delta z$ in the modified system, respectively. We then have:

$$\begin{aligned}
\delta\Omega_{\text{PB}} &= \frac{\varepsilon}{4\pi} \int_0^d dz \left(\frac{d\Psi}{dz} \right) \delta \left(\frac{d\Psi}{dz} \right) + k_B T \int_0^d dz \sum_i \delta c_i \ln \frac{c_i}{\zeta} \\
&\quad + \delta z \left[\frac{\varepsilon}{8\pi} \left(\frac{d\Psi}{dz} \right)^2 + k_B T \sum_i c_i \left(\ln \frac{c_i}{\zeta} - 1 \right) \right]_{z=z_0}
\end{aligned} \tag{A2}$$

The first term can be integrated by parts. With the conventions described above, the boundary terms can be written as follows:

$$\begin{aligned}
&\Psi \delta \left. \frac{d\Psi}{dz} \right|_0^{z_0} + \Psi \delta \left. \frac{d\Psi}{dz} \right|_{z_0}^d = \\
&= \Psi(z_0) \left[\frac{d\Psi_{\text{new}}}{dz}(z_0) - \frac{d\Psi}{dz}(z_0) - \frac{d\Psi_{\text{new}}}{dz}(z_0 + \delta z) + \frac{d\Psi}{dz}(z_0) \right] \\
&= -\Psi(z_0) \frac{d^2\Psi}{dz^2}(z_0) \delta z
\end{aligned} \tag{A3}$$

where use of the boundary conditions at $z = 0$ and $z = d$ has been made. Using this relation and the Poisson equation (5), we obtain:

$$\begin{aligned}
\delta\Omega_{\text{PB}} &= \delta z \left[\sum_i e_i \Psi c_i + \frac{\varepsilon}{8\pi} \left(\frac{d\Psi}{dz} \right)^2 + k_B T \sum_i c_i \left(\ln \frac{c_i}{\zeta} - 1 \right) \right]_{z_0} \\
&\quad + \int_0^d dz \sum_i \delta c_i \left[e_i \Psi + k_B T \ln \frac{c_i}{\zeta} \right]
\end{aligned} \tag{A4}$$

To compute $\delta\Delta\Omega$, $\Delta\Omega$ can be separated to the following three terms:

$$\begin{aligned}
\Delta\Omega &= \frac{1}{2} k_B T \sum_{i,j} \int_0^{z_0} dz \int_0^{z_0} dz' c_i(z) c_j(z') B_{ij}(z' - z) \\
&\quad + \frac{1}{2} k_B T \sum_{i,j} \int_{z_0}^d dz \int_{z_0}^d dz' c_i(z) c_j(z') B_{ij}(z' - z) \\
&\quad + k_B T \sum_{i,j} \int_0^{z_0} dz \int_{z_0}^d dz' c_i(z) c_j(z') B_{ij}(z' - z)
\end{aligned} \tag{A5}$$

The variation of c_i in these three terms gives:

$$\delta\Delta\Omega_1 = k_B T \sum_{i,j} \int_0^d dz \int_0^d dz' c_i(z) \delta c_j(z') B_{ij}(z' - z) \tag{A6}$$

The variation of the third term in Eq. (A5) gives two additional contributions, one from the variation of $B(z' - z)$ under the insertion of the ‘slice’ at z_0 :

$$\delta\Delta\Omega_2 = \delta z \cdot k_B T \sum_{i,j} \int_0^{z_0} dz \int_{z_0}^d dz' c_i(z) c_j(z') \frac{dB_{ij}}{dz}(z' - z) \tag{A7}$$

and the other from the integration over the ‘slice’ itself:

$$\delta\Delta\Omega_3 = \delta z \cdot k_B T \sum_{i,j} \int_0^d dz c_i(z_0) c_j(z) B_{ij}(z - z_0) \tag{A8}$$

Summing up all the contributions to $\delta\Omega$ we have:

$$\begin{aligned}
\delta\Omega &= \delta\Omega_{\text{PB}} + \delta\Delta\Omega_1 + \delta\Delta\Omega_2 + \delta\Delta\Omega_3 \\
&= \delta z \sum_i c_i(z_0) \times \left\{ \frac{\varepsilon}{8\pi} \left(\frac{d\Psi}{dz} \right)^2 (z_0) + e_i \Psi(z_0) + k_B T \left[\ln \frac{c_i(z_0)}{\zeta} - 1 \right] + k_B T \sum_j \int_0^d dz c_j(z) B_{ij}(z - z_0) \right\} \\
&\quad + \int_0^d dz \sum_i \delta c_i(z) \times \left\{ e_i \Psi(z) + k_B T \ln \frac{c_i(z)}{\zeta} + k_B T \sum_j \int_0^d dz' c_j(z') B_{ij}(z' - z) \right\} \\
&\quad + \delta z k_B T \sum_{ij} \int_0^{z_0} dz \int_{z_0}^d dz' c_i(z) c_j(z') \frac{dB_{ij}}{dz}(z' - z)
\end{aligned} \tag{A9}$$

Using the equilibrium equation (7) this reduces to:

$$\begin{aligned}
-\frac{\delta\Omega}{\delta z} &= k_B T \sum_i c_i(z_0) - \frac{\varepsilon}{8\pi} \left(\frac{d\Psi}{dz} \right)^2 \Big|_{z_0} \\
&\quad - k_B T \sum_{ij} \int_0^{z_0} dz \int_{z_0}^d dz' c_i(z) c_j(z') \frac{dB_{ij}}{dz}(z' - z)
\end{aligned} \tag{A10}$$

This result can be readily generalized to the case of several ion species, as in Eq. (18).

-
- ¹ J. Israelachvili, *Intermolecular and Surface Forces*, 2nd ed. (Academic Press Inc., New York, 1991).
- ² G. Gouy, *J. Phys. (France)* **9**, 457 (1910).
- ³ D. L. Chapman, *Philos. Mag.* **25**, 475 (1913).
- ⁴ P. Debye and E. Hückel, *Physik* **24**, 185 (1923).
- ⁵ P. Debye and E. Hückel, *Physik* **25**, 97 (1924).
- ⁶ D. Andelman, in *Handbook of Physics of Biological Systems*, edited by R. Lipowsky and E. Sackmann (Elsevier Science, Amsterdam, 1994), Vol. I, Chap. 12, p. 603.
- ⁷ E. J. W. Verwey and J. T. G. Overbeek, *Theory of the Stability of Lyophobic Colloids* (Elsevier, Amsterdam, 1948).
- ⁸ S. Alexander *et al.*, *J. Chem. Phys.* **80**, 5776 (1984).
- ⁹ F. Oosawa, *Polyelectrolytes* (Marcel Dekker, New York, 1971).
- ¹⁰ J. L. Barrat and J. F. Joanny, *Adv. Chem. Phys.* **XCIV**, 1 (1996).
- ¹¹ D. Harries, S. May, W. M. Gelbart, and A. Ben-Shaul, *Biophys. J.* **75**, 159 (1998).
- ¹² L. Blum and D. Henderson, in *Fundamentals of Inhomogeneous Fluids*, edited by D. Henderson (Marcel Dekker, Inc., New York, 1992), Chap. 6, pp. 239–276, and references therein.
- ¹³ R. Kjellander and S. Marčelja, *J. Chem. Phys.* **82**, 2122 (1985).
- ¹⁴ R. Kjellander, *J. Chem. Phys.* **88**, 7129 (1988).
- ¹⁵ S. Levine, C. W. Outhwaite, and L. B. Bhuiyan, *J. Electroanal. Chem.* **123**, 105 (1981).
- ¹⁶ C. W. Outhwaite and L. B. Bhuiyan, *J. Chem. Soc. Faraday Trans. 2* **79**, 707 (1983).
- ¹⁷ M. J. Stevens and M. O. Robbins, *Europhys. Lett.* **12**, 81 (1990).
- ¹⁸ L. Guldbrand, B. Jönsson, H. Wennerström, and P. Linse,

- J. Chem. Phys.* **80**, 2221 (1984).
- ¹⁹ R. Kjellander, T. Åkesson, B. Jönsson, and S. Marčelja, *J. Chem. Phys.* **97**, 1424 (1992).
- ²⁰ H. Greberg, R. Kjellander, and T. Åkesson, *Mol. Phys.* **92**, 35 (1997).
- ²¹ R. R. Netz and H. Orland, *Europhys. Lett.* **45**, 726 (1999).
- ²² R. R. Netz and H. Orland, *Europhys. J. E.* **1**, 203 (2000).
- ²³ I. Borukhov, D. Andelman, and H. Orland, *Phys. Rev. Lett.* **79**, 435 (1997).
- ²⁴ I. Borukhov, D. Andelman, and H. Orland, *Electrochim. Acta* (in press).
- ²⁵ D. B. Lukatsky and S. A. Safran, *Phys. Rev. E.* **60**, 5848 (1999).
- ²⁶ L. Lue, N. Zoeller, and D. Blankschtein, *Langmuir* **15**, 3726 (1999).
- ²⁷ A. P. Lyubartsev and A. Laaksonen, *Phys. Rev. Lett.* **55**, 5689 (1997).
- ²⁸ S. Marčelja, *Nature* **385**, 689 (1997).
- ²⁹ S. Marčelja, *Period. Biol.* **100**, 7 (1998).
- ³⁰ S. Marčelja, *Colloid Surface A* **130**, 321 (1997).
- ³¹ R. Kjellander, A. P. Lyubartsev and S. Marčelja, submitted to *J. Chem. Phys.*
- ³² F. Otto and G. N. Patey, *J. Chem. Phys.* **112**, 8939 (2000).
- ³³ Y. Burak and D. Andelman, *Phys. Rev. E.* (in press).
- ³⁴ R. R. Netz, private communication.
- ³⁵ S. Marčelja, private communication.
- ³⁶ S. L. Carnie and D. Y. C. Chan, *J. Chem. Phys.* **74**, 1293 (1981).
- ³⁷ In Refs. 28–30 there was an error in the inclusion of the hydration pressure, making it much smaller than its real value. The corrected data, kindly provided to us by S. Marčelja, is used in the comparison of the present work with the AHNC results.
- ³⁸ E. Guàrdia and J. A. Padró, *J. Chem. Phys.* **104**, 7219 (1996).
- ³⁹ J. C. Neu, *Phys. Rev. Lett.* **82**, 1072 (1999).
- ⁴⁰ J. E. Sader and D. Y. C. Chan, *J. Colloid Interface Sci.*

- 213**, 268 (1999).
- ⁴¹ R. M. Pashley, *J. Colloid Interface Sci.* **80**, 153 (1981).
- ⁴² R. M. Pashley and J. N. Israelachvili, *J. Colloid Interface Sci.* **101**, 511 (1984).
- ⁴³ S. Marčelja, *Langmuir* (in press).
- ⁴⁴ J. Israelachvili and H. Wennerström, *Nature* **379**, 219 (1996).

Fig. 1: Short-range effective potential between Na^+ ion pairs, adapted from Ref. 27 using simulations in a bulk NaCl aqueous solution of concentration 0.55M, at room temperature³⁵. The potential is shown in units of $k_B T$, as a function of the distance between the ion centers. The Coulomb interaction is subtracted to show only the short-range hydration effect due to the water molecules. For ion-ion separations below 2.9\AA a hard core interaction is taken.

Fig. 2: Schematic description of the pair potential model. An aqueous ionic solution confined between two charged plates in (a) is replaced by ions in a continuum dielectric medium with electrostatic and short-range interactions $u_{ij}(r) = u_{ij}(|\mathbf{r}|)$ in (b). The coordinates $z = 0$ and $z = d$ designate the contact positions of the ions with the plates. The distance of closest approach is equal to $d_{\text{hc}}/2$, where d_{hc} is the hard-core diameter of the ions.

Fig. 3: The effective layer-layer interaction $B(z)$ in a planar geometry, as obtained from the potential of Fig. 1 using Eq. (8) (solid line). The oscillating structure of the radial potential shown in Fig. 1 is apparent in the secondary minima of $B(z)$.

Fig. 4: Counterion density profile (solid line) obtained from numerical solution of Eq. 7 with the hydration interaction as of Fig. 3, plotted on a semi-log plot. The bulk ion density is $c_b = 0.025\text{M}$ and the surface charge is $|\sigma| = 0.333\text{C/m}^2$. The dielectric constant is $\epsilon = 78$ and the temperature is 298K. The distance between the plates is $d = 50\text{\AA}$. The density profile is symmetric about the mid-plane at $z = 25\text{\AA}$. The dotted line shows the corresponding density profile obtained from the PB equation. The symbols ('x') show the density profile obtained in the AHNC approximation, using the same parameters.

Fig. 5: The ratio of the positive ion density obtained from Eq. (7) and the value obtained from PB theory, for surface charges $|\sigma| = 0.333\text{C/m}^2$ (dashed line), 0.1C/m^2 (solid line) and 0.0333C/m^2 (dotted line). All other parameters are as in Fig. 4.

Fig. 6: The ratio between the positive ion density obtained from Eq. (7) and its PB value, for plate separations d equal to (a) 50\AA (solid line), 35\AA (dashed line), 20\AA (solid line), (b) 10\AA and (c) 5\AA . All other parameters are as in Fig. 4. Each curve is shown between the plate at $z = 0$ and the mid-plane $z = d/2$.

Fig. 7: (a) Pressure between two plates with surface charge $|\sigma| = 0.333\text{C/m}^2$, as a function of the plate separation d , on a semi-log plot. All the parameters are as in Fig. 4. The solid line shows the overall pressure P obtained from Eq. (22). The dashed line shows the contribution P_m resulting from the mid-plane density and the dotted line shows the PB pressure. (b) The same curves on a linear scale, in the region where the overall pressure becomes negative, *i.e.*, attractive.

Fig. 8: The repulsive pressure between two plates with surface charge $|\sigma| = 0.119\text{C/m}^2$, as a function of the plate separation d . All other parameters are as in Fig. 4. The solid line shows the overall pressure P , the dashed line shows the contribution P_m of the mid-plane density, and the dotted line shows the results of PB theory.

Fig. 9: Comparison between the pressure obtained (a) in our model and (b) in the AHNC approximation, using the same short-range hydration potential (solid lines). All the parameters are as in Fig. 7 ($|\sigma| = 0.333\text{C/m}^2$). The pressure is shown as a function of the plate separation d . A semi-logarithmic scale is used in the main plots and a linear scale is used in the insets. In (a) the dotted line shows the PB pressure. In (b) the dotted line shows the pressure obtained in the AHNC approximation when the ion-ion interaction includes only the hard core and the electrostatic interactions.

Fig. 10: Comparison between the pressure obtained in our model (solid line) and the AHNC approximation (dashed line), for a surface charge $|\sigma| = 0.119\text{C/m}^2$. All the parameters are as in Fig. 8. The pressure is shown as a function of the inter-plate separation d using a semi-logarithmic plot. The dotted line shows the PB pressure.

Fig. 11: The hydration pressure P_{hyd} as a function of the plate separation d (solid line). All the parameters are as in Fig. 4. The dashed line shows the approximation to P_{hyd} obtained by replacing the ion density in the integral of Eq. (29) by the PB ion density.

Fig. 12: Repulsive pressure between two plates with surface charge $|\sigma| = 0.25\text{C/m}^2$, as a function of the plate separation d , using a linear plot (solid line). All other parameters are as in Fig. 4. The pressure is compared with the PB pressure curve fitted to the large separation behavior, with $|\sigma_{\text{eff}}| \simeq 0.09\text{C/m}^2$ (dashed line).

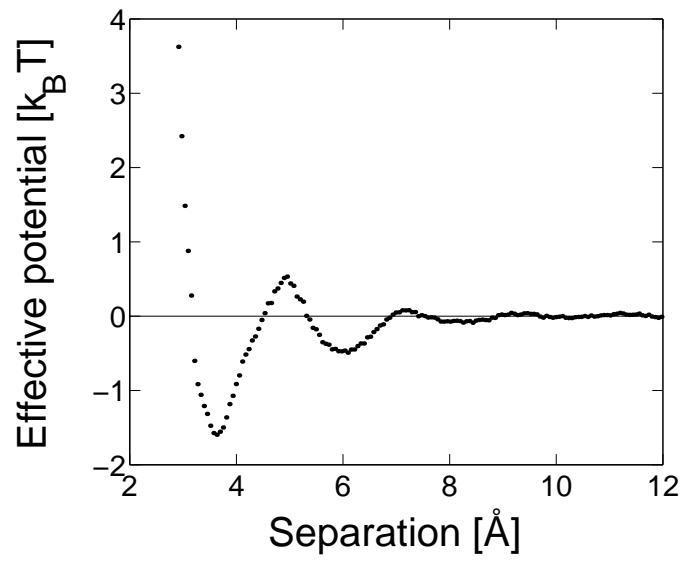


Fig. 1

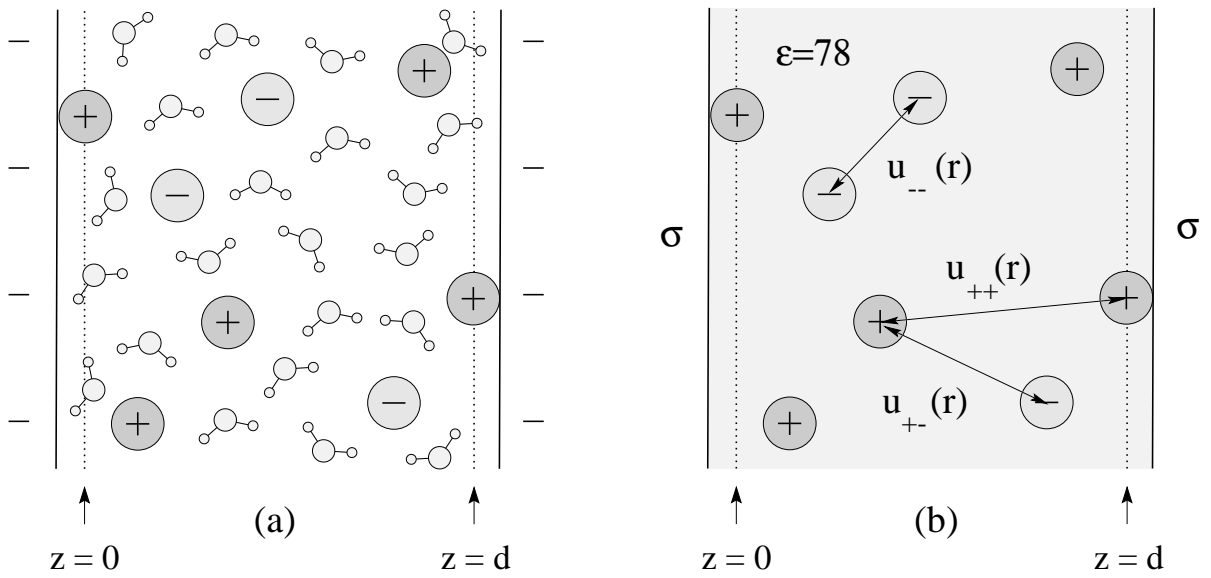


Fig. 2

Y.Burak + D.Andelman

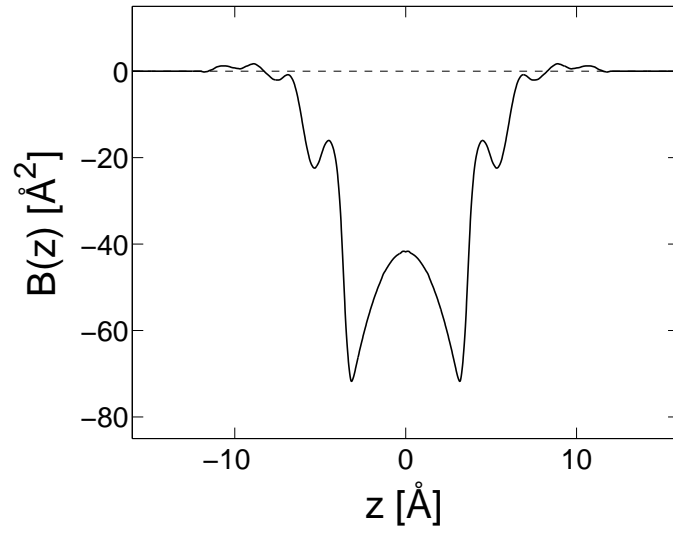


Fig. 3

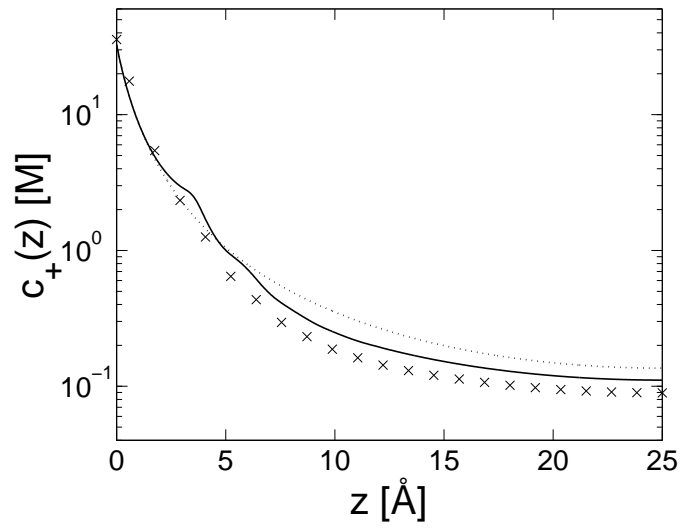


Fig. 4

Y.Burak + D.Andelman

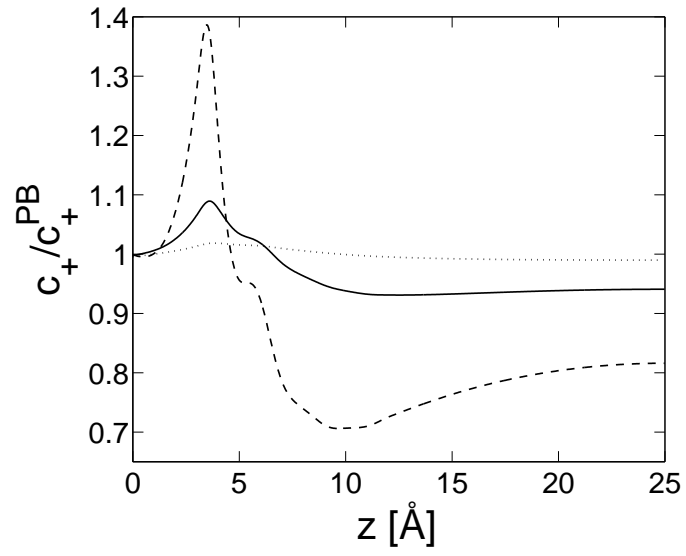


Fig. 5

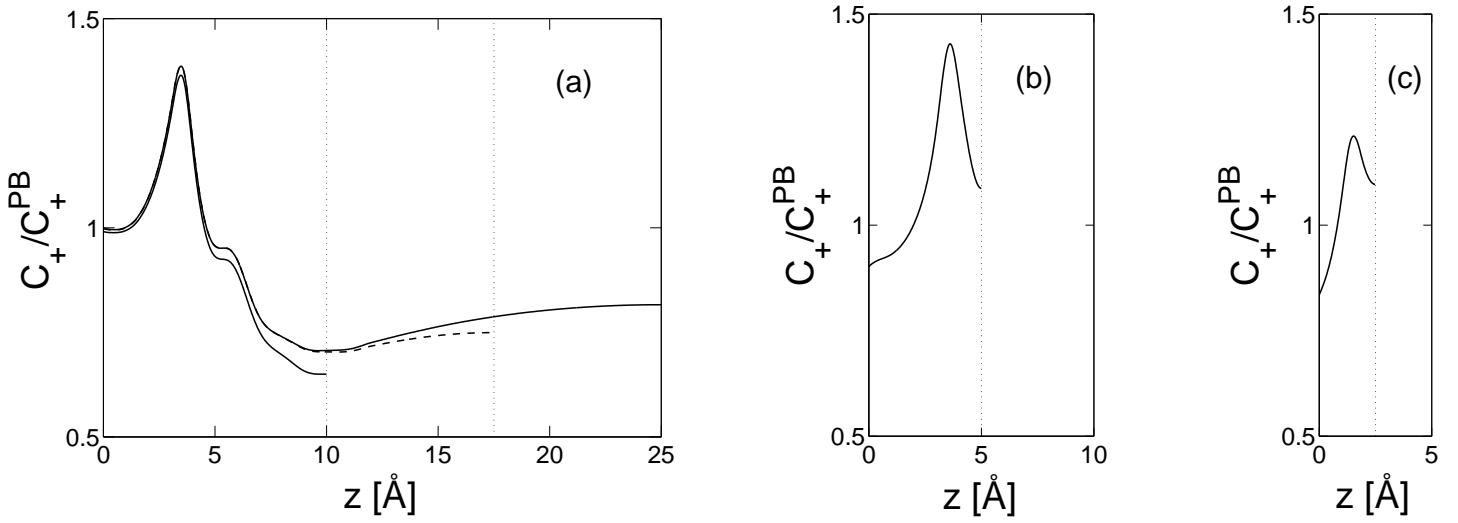


Fig. 6

Y.Burak + D.Andelman

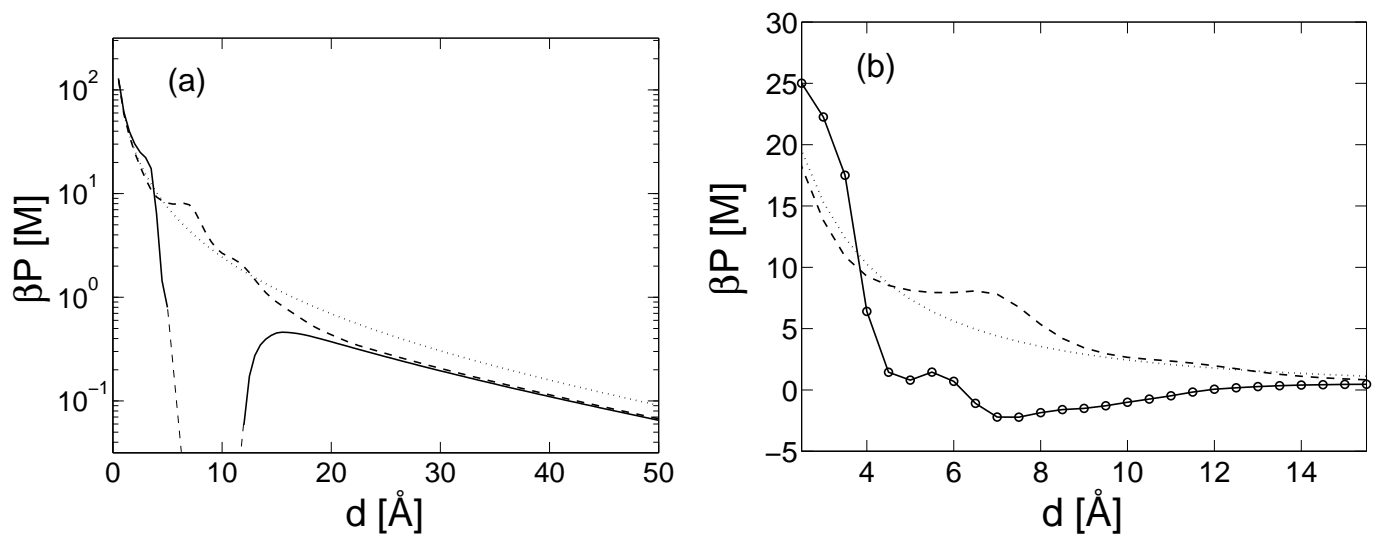


Fig. 7

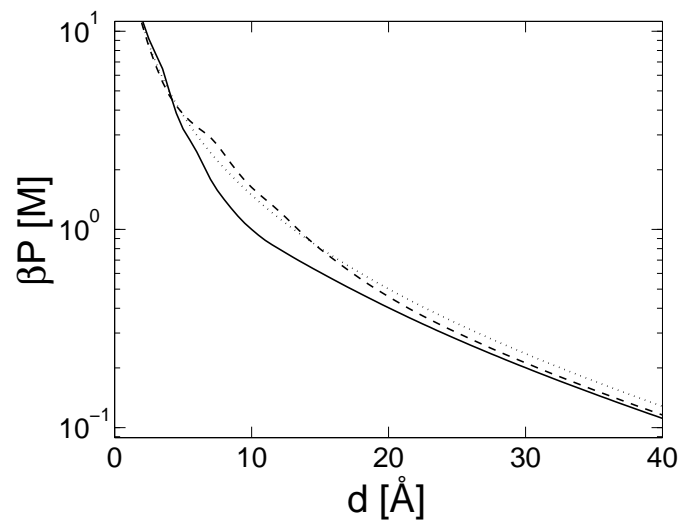


Fig. 8

Y.Burak + D.Andelman

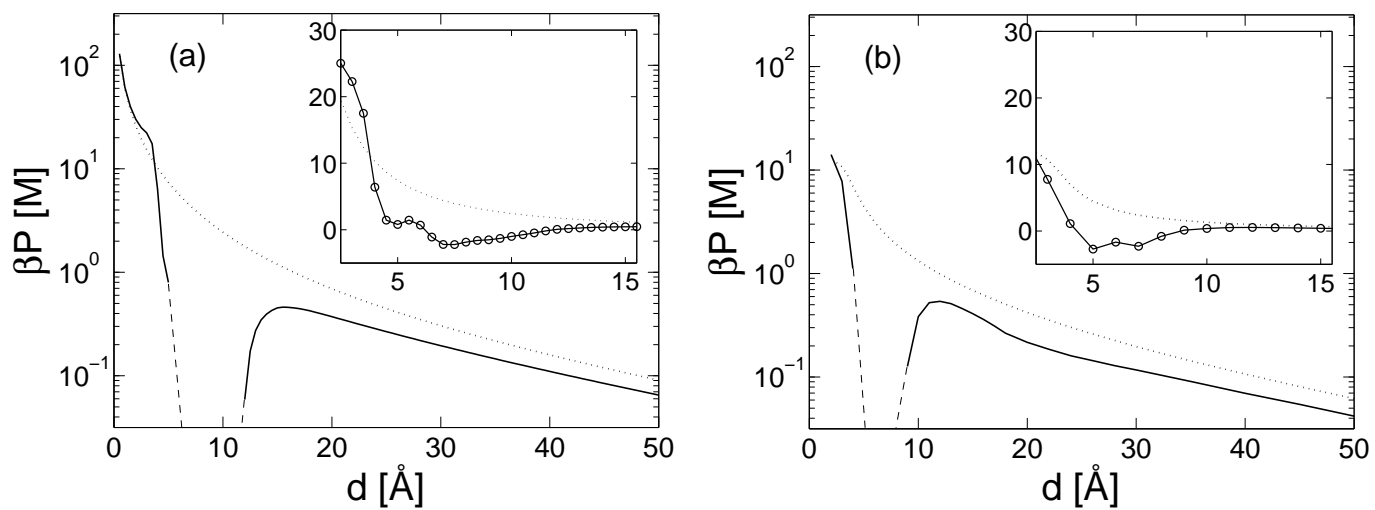


Fig. 9

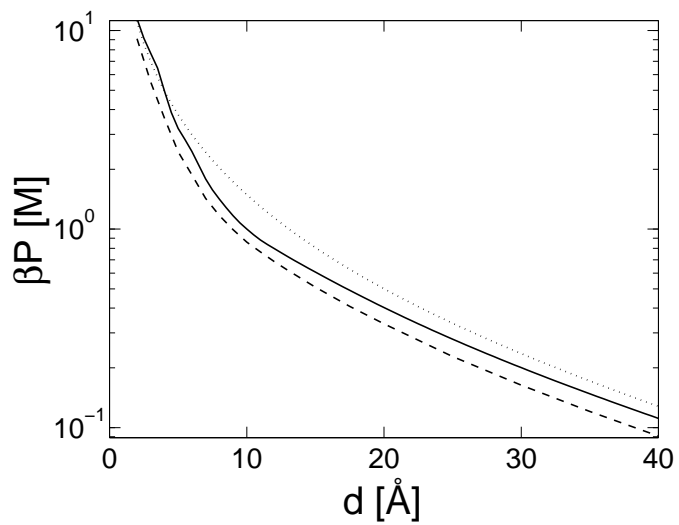


Fig. 10

Y.Burak + D.Andelman

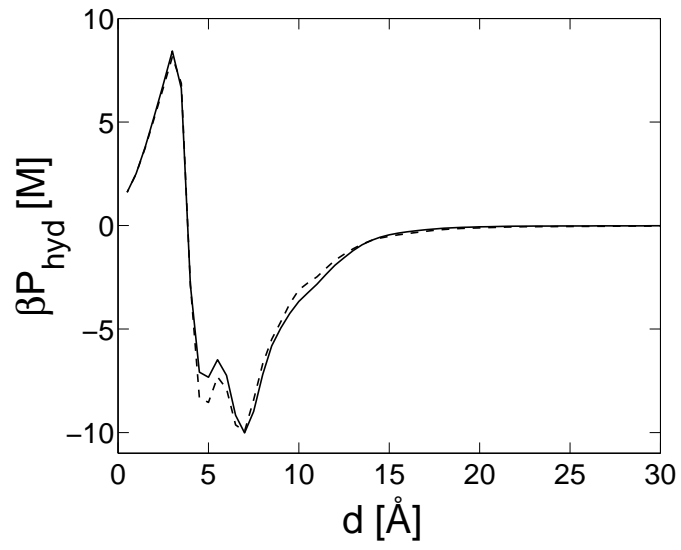


Fig. 11

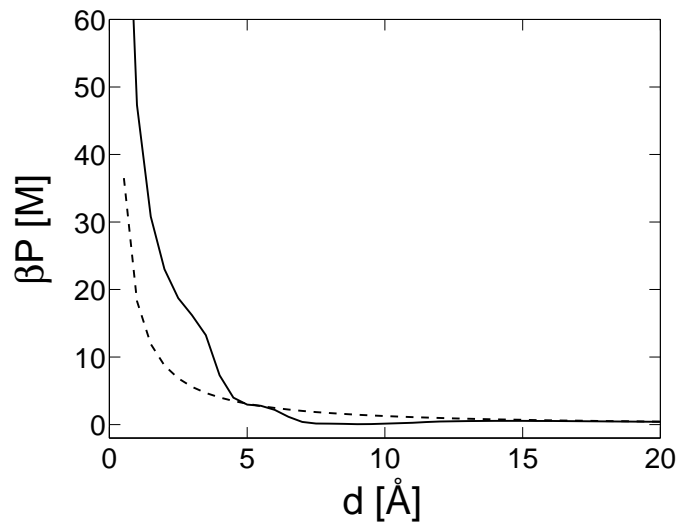


Fig. 12

Y.Burak + D.Andelman